Editors' Suggestion

Perturbed Nonlinear Evolution of Optical Soliton Gases: Growth and Decay in Integrable Turbulence

Loic Fache, François Copie, Pierre Suret, and Stéphane Randoux*
Univ. Lille, CNRS, UMR 8523—PhLAM—Physique des Lasers Atomes et Molécules, F-59 000 Lille, France

(Received 17 March 2025; accepted 16 September 2025; published 8 October 2025)

We present optical fiber experiments investigating the perturbed, nonintegrable evolution of soliton gases (SGs) under weak linear damping and gain. By measuring the amplitude and phase of the optical field in a recirculating loop, we determine the spectral distribution of SGs at various propagation distances. We demonstrate that a SG, initially prepared as a soliton condensate with a Weyl distribution, undergoes significant changes in its spectral distribution due to dissipation. Specifically, weak gain leads to the emergence of a bichromatic SG, while weak damping results in a SG with a semicircular spectral distribution at long propagation distances. These observed dissipation-driven changes in the SG's spectral characteristics are not explained by existing hydrodynamic or kinetic theories.

DOI: 10.1103/hwpr-628r

Integrable turbulence (IT) refers to both a physical phenomenon and a theoretical framework for studying the dynamics of nonlinear random waves in systems governed by integrable equations, such as the Korteweg-de Vries (KdV) equation or the one-dimensional nonlinear Schrödinger equation (1D NLSE) [1–9]. In contrast to wave turbulence [10–13], which addresses the behavior of out-of-equilibrium, nonlinear random dispersive waves in nonintegrable systems, the theoretical framework underlying IT is the inverse scattering transform (IST) method [14,15]. This distinction provides a relevant perspective on the analysis of large-scale, emergent hydrodynamic phenomena in integrable systems, where soliton gas (SG) serves as a central concept [16–20].

SG can be defined as an infinite ensemble of interacting solitons with randomly distributed amplitudes, velocities, and positions [16,17,20]. The integrable dynamics, constrained by the existence of an infinite number of conserved quantities, prevent SGs from achieving relaxation to the classical Gibbs ensembles. Instead SGs exhibit local nonthermal stationary states, the so-called generalized Gibbs ensembles, which play a fundamental role in generalized hydrodynamics (GHD), the hydrodynamic theory of many-body quantum and classical integrable systems [21–25]. Currently, the out-of-equilibrium evolution of SGs represents an active area of research, explored using the spectral kinetic theory of SGs and GHD [18,20,22,24].

Despite several experimental observations of SGs across various physical systems [3,26–31], only a few experimental studies have questioned the validity of the spectral kinetic theory of SGs in a quantitative way [32–34]. Several experiments have demonstrated that while perturbative higher-order effects are inevitably present, they break integrability to such a negligible degree that the predictions of kinetic theory still align closely with experimental results [32,33]. In contrast, other experiments have demonstrated that even small perturbative higher-order effects can significantly alter integrable dynamics, leading to unexpected behaviors not anticipated at the theoretical level [34]. For example, a KdV soliton condensate has been shown to emerge spontaneously as a result of weak dissipation in a nonlinear electrical transmission line [34].

In this Letter, we present experiments investigating the perturbed, nonintegrable evolution of optical SGs, which reveal unexpected and remarkable changes in their spectral, IST properties. Using a recirculating optical fiber loop that allows precise control of either optical gain or losses, we examine the growth and decay of IT in SG experiments, accurately described by the focusing 1D NLSE with a weak linear gain or damping term [35–37]. Our experiments reveal that the SG, initially prepared as a soliton condensate characterized by the Weyl distribution, undergoes significant changes in its spectral distribution due to dissipation. We find that a small amount of optical gain leads to the emergence of a bichromatic SG. On the other hand, small damping is found to alter the geometric shape of the IST spectrum, resulting in a semicircular spectral configuration at long evolution time. The dissipation-driven changes observed experimentally in the spectral characteristics of the optical SGs are not explained by existing hydrodynamic or kinetic theories of SG.

Our experimental setup is depicted schematically in Fig. 1. It comprises a recirculating fiber loop constructed from ∼8 km of single-mode fiber (SMF), which is closed upon itself using a 90/10 fiber coupler. This coupler is configured to recirculate 90% of the optical power. The optical signal circulates in the clockwise direction, and at

*Contact author: stephane.randoux@univ-lille.fr

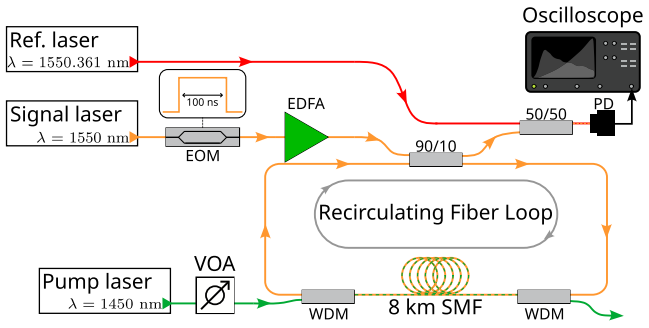

FIG. 1. Experimental setup. A SG, initially in the form of a 100 ns-long flat-top pulse at 1550 nm, perturbed by optical noise, propagates through a recirculating fiber loop where the optical gain or loss rate can be precisely controlled through Raman amplification using a 1450 nm pump laser. Measurement of the amplitude and the phase of the optical signal is made using a heretodyne technique where the optical signal at the output of the fiber loop is mixed with a single-frequency laser at 1550.361 nm.

each round trip, 10% of the circulating power is extracted and directed to a photodetector (PD) connected to a fast oscilloscope with a sampling rate of 160 GSa/s and a bandwidth of 65 GHz. The overall detection bandwidth of the oscilloscope and the PD is 32 GHz. The periodic extraction of light at each round trip within the recirculating fiber loop enables stroboscopic monitoring of the wave field's evolution every 8 km. The signals recorded by the oscilloscope are subsequently processed numerically to generate space-time diagrams that illustrate the dynamics of the wave field over hundreds of round trips inside the fiber loop [33,38,39].

A typical experiment involves circulating a long, flat-top pulse (∼100 ns duration) for 400 to 800 round trips in the fiber loop, corresponding to total propagation distances of ∼3200 km to ∼6400 km. The flat-top pulse is generated using a fast electro-optic modulator (EOM) and is perturbed by a small amount of optical noise introduced by an Erbium-doped amplifier prior to the pulse's injection into the fiber loop, see Fig. 1. As a result of the process of modulation instability, the perturbed flat-top pulse evolves into a fully randomized bound state SG [29,33,40–43].

The mean gain or loss of the optical signal over hundreds of round trips in the fiber loop can be precisely controlled through Raman amplification, using a counterpropagating 1450 nm pump laser coupled into and out of the loop via wavelength division multiplexers (WDMs), as shown in Fig. 1. By carefully adjusting the optical power of the pump laser using a variable optical attenuator (VOA), we performed experiments where the mean power of the optical SGs is set to exponentially increase or decay at a given rate, allowing us to explore both growing and decaying stages of IT [35,36].

Capturing the changes in the IST spectrum experienced by SGs during propagation is a significant challenge in optics, as it requires simultaneous measurement of both the amplitude and phase of the optical field. In this work, we address this challenge using a heterodyne technique. Specifically, the optical signal at the output of the recircu lating fiber loop is mixed with a single-frequency reference field that is detuned by approximately 45 GHz (equivalently 0.361 nm) from the central frequency of the optical signal. As illustrated in Fig. 1, the optical signal and the detuned reference field are combined using a 50/50 fiber coupler, with the output directed to a fast photodetector (PD). The reconstruction of the optical field's amplitude and phase employs conventional signal processing techniques that are described in the Supplemental Material [44].

Focusing first on experiments involving decaying IT, Fig. 2(b) illustrates the space-time evolution of the optical wave field power, experimentally observed as the mean power $P(z)$ of the flat-top pulse decreases from $P_0 \sim 11.5$ mW to ∼2 mW over a propagation distance of ∼3200 km [see Fig. 2(a)]. At a qualitative level, the experimentally reconstructed space-time diagram over a narrow 5 ns time window closely resembles the space-time patterns typically associated with the noise-driven modulation instability of plane waves in systems governed by the focusing 1D NLSE [39,45–50].

As shown in Fig. 2(e), the dynamical features observed in our experiment are quantitatively well described by numerical simulations of the following 1D NLSE with a small linear damping term:

$$i\frac{\partial A}{\partial z} = \frac{\beta_2}{2}\frac{\partial^2 A}{\partial T^2} - \gamma|A|^2 A - i\frac{\alpha_{\text{eff}}}{2}A. \tag{1}$$

$A(z,T)$ represents the complex envelope of the electric field that slowly varies in physical space z and time T. The Kerr coefficient of the fiber is $\gamma = 1.3\ \text{W}^{-1}\,\text{km}^{-1}$. The group velocity dispersion coefficient is $\beta_2 = -22\ \text{ps}^2\,\text{km}^{-1}$. $\alpha_{\text{eff}} > 0$ represents the effective power decay rate of the circulating field. In the experiment presented in Figs. 2(a) and 2(b), its value is $\alpha_{\text{eff}} \sim 5.8 \times 10^{-4}\ \text{km}^{-1}$ or equivalently ∼0.0025 dB/km.

Although the space-time diagrams in Figs. 2(b) and 2(e) might suggest that dissipation has a negligible effect on the noise-driven destabilization of the initial flat-top pulse, we now show that the discrete IST spectra of the optical SG reveal distinct features introduced by dissipation to the dynamics. For the computation of the discrete IST spectra, we first introduce the following dimensionless form of the focusing 1D NLSE [37,48]:

$$i\psi_t + \psi_{xx} + 2|\psi|^2\psi + i\epsilon\psi = 0, \tag{2}$$

which is obtained from Eq. (1) using the following transformations: $\psi = A/\sqrt{P_0}$, $x = T\sqrt{\gamma P_0/|\beta_2|}$, $t = \gamma P_0 z/2$, $\epsilon = \alpha_{\text{eff}}/(\gamma P_0)$ [33].

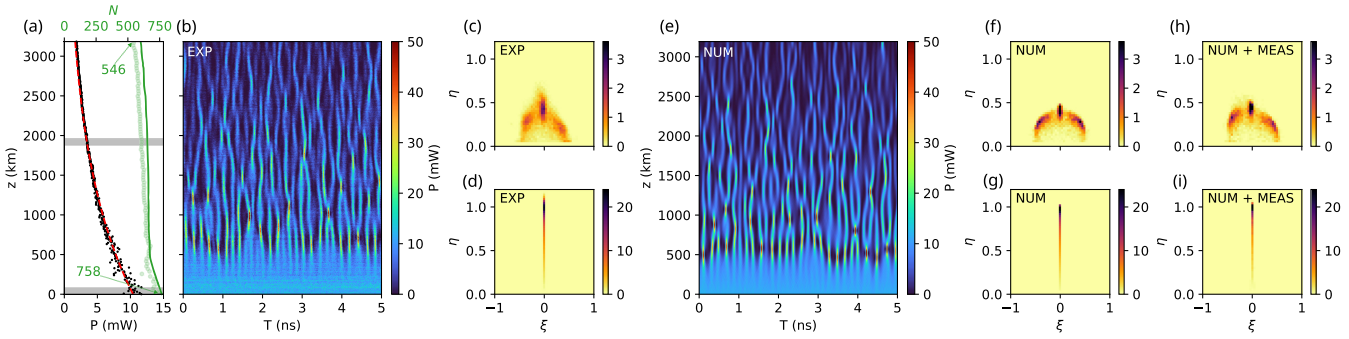

FIG. 2. Experiments and numerical simulations showing the evolution of an optical SG in a recirculating fiber loop in the presence of small damping. (a) The black points represent the measured power of the SG as a function of the propagation distance z. The red line represents the evolution of the optical power computed in numerical simulations. The green points (resp. line) represent the number of discrete eigenvalues λ_i measured in the experiment (resp. computed in numerical simulations) as a function of z. (b) Space-time evolution of the optical power of the SG measured in the experiment. (c) DOS of the optical SG measured at $z = 1920$ km in the upper complex plane. (d) DOS of the initial condition. (e) Same as (b) but from numerical simulations of Eq. (1) with $\gamma = 1.3\ \mathrm{W^{-1}\,km^{-1}}$, $\beta_2 = -22\ \mathrm{ps^2\,km^{-1}}$, $\alpha_{\mathrm{eff}} \sim 5.8 \times 10^{-4}\ \mathrm{km^{-1}}$, $P(z=0) = P_0 = 11.5$ mW. (f),(g) Same as (c) and (d) but computed from simulations reported in (e). (h),(i) Same as (f) and (g) but including noise and finite bandwidth effects in the heterodyne measurement, see Supplemental Material [44] for details.

Within the IST formalism, the non-self-adjoint Zakharov-Shabat eigenvalue problem that is associated with Eq. (2) for $\epsilon = 0$ reads [51]

$$\hat{\mathcal{L}}\Phi = \lambda\Phi, \qquad \hat{\mathcal{L}} = \begin{pmatrix} -i\partial_x & -i\psi \\ -i\psi^* & i\partial_x \end{pmatrix}. \tag{3}$$

$\mathbf{\Phi}(x,\lambda)$ is a vector wave function. $\lambda \in \mathbb{C}$ represent the eigenvalues composing the discrete spectrum associated with the soliton content of the field $\psi = \psi(x,t)$ that is measured at some given evolution time t (equivalently at some given propagation distance z in the experiment). Each soliton in a soliton gas, consisting of an ensemble of N solitons, is characterized by a discrete eigenvalue $\lambda_j = \xi_j + i\eta_j (j = 1, \ldots, N)$ of the spectrum of the linear operator $\hat{\mathcal{L}}$, where ξ_j and η_j parameterize the velocity and amplitude of each soliton, respectively. Importantly, integrable dynamical evolution [implying $\epsilon = 0$ in Eq. (2)] entails an isospectral property, meaning that all the discrete eigenvalues λ_j remain invariant with respect to the evolution variable t.

The discrete IST spectra of the optical SG are computed from the normalized experimental complex fields $\psi = A/\sqrt{P_0}$ by solving numerically Eq. (3) using the Fourier collocation method described in Ref. [51]. The output of this numerical calculation is an ensemble of several hundreds of discrete, complex-valued eigenvalues λ_j that are located in a bounded region of the upper complex plane. Given the large number of discrete eigenvalues that are found from nonlinear spectral analysis, we follow the approach used in the kinetic theory of SG and compute the so-called density of states (DOS) $f(\lambda; x, t)$ of the SG.

The DOS $f(\lambda; x, t)$, where $\lambda = \xi + i\eta$, represents the density of soliton states in the phase space, i.e., $f d\xi d\eta dx$ is the number of solitons contained in a portion of SG with the complex spectral parameter $\lambda \in [\xi, \xi + d\xi] \times [\eta, \eta + d\eta]$ over the space interval $[x, x + dx]$ at time t (corresponding to the position z in the fiber loop experiment). Given that the optical SG is spatially homogeneous, the DOS represents the probability density function of the complex-valued discrete eigenvalues normalized in such a way that $\int_{-\infty}^{+\infty} d\xi \int_0^{+\infty} d\eta f(\lambda) = N/\Delta x$, where N represents the number of eigenvalues found in the upper complex plane and Δx represents the spatial extent of the gas [19,30].

In practice, the experimental DOS is computed not from a single flat-top pulse, but from three identical flat-top pulses, each evolving independently within the fiber loop during the same experimental run. Assuming minimal variation in the IST spectra over short propagation distances, the DOS is calculated by averaging the IST spectra of the three pulses collected over a 80 km propagation span, as highlighted by the gray-shaded regions in Fig. 2(a). The statistical computation of the DOS involves an ensemble of ~23 200 (resp. ~18 300) discrete eigenvalues at $z = 0$ km (resp. $z = 1920$ km).

Figure 2(d) shows the DOS of the flat-top pulse perturbed by small optical noise that is taken as the initial condition in the experiment ($z = 0$ km). As it can be easily anticipated from previous works [40], we find that the measured DOS is very well fitted by the Weyl distribution $f_W(\eta) = \eta/(\pi\sqrt{1-\eta^2})$ located along the vertical imaginary axis $\xi = 0$ [see also Fig. 4(a)]. Because of dissipation, the isospectrality condition characteristic of integrable dynamics is not expected to be satisfied in our experiment. However, since the damping effects are small [$\epsilon \simeq 0.038$ in Eq. (2)], IST analysis remains a relevant tool for examining the evolution of the optical SG. Figure 2(c), computed at $z \sim 1900$ km, shows that optical damping transforms the

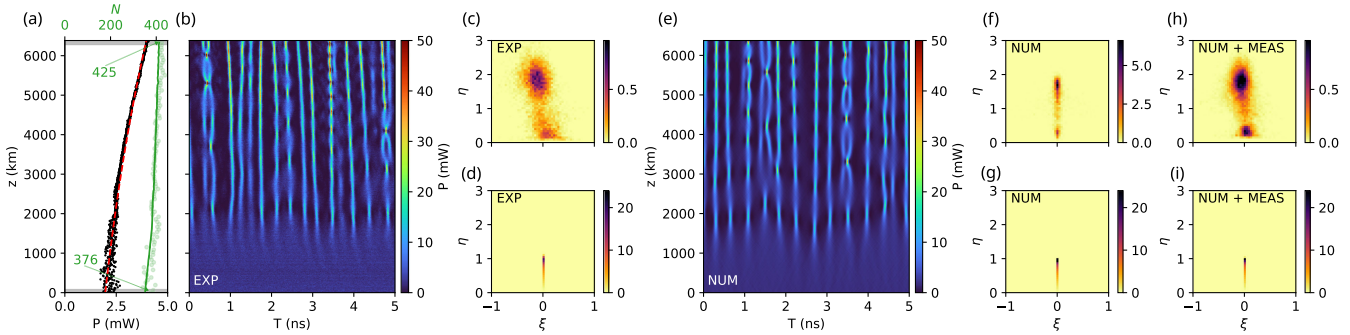

FIG. 3. Experiments and numerical simulations showing the evolution of an optical SG in a recirculating fiber loop in the presence of small gain. (a) The black points represent the measured power of the SG as a function of the propagation distance z. The red line represents the evolution of the optical power computed in numerical simulations. The green points (resp. line) represent the number of discrete eigenvalues λ_i measured in the experiment (resp. computed in numerical simulations) as a function of z. (b) Space-time evolution of the optical power of the SG measured in the experiment. (c) DOS of the optical SG measured at $z = 6320$ km in the upper complex plane. (d) DOS of the initial condition. (e) Same as (b) but from numerical simulations of Eq. (1) with $\alpha_{\text{eff}} \sim -1.1 \times 10^{-4}$ km^{-1}, $P(z = 0) = P_0 = 2$ mW. (f),(g) Same as (c) and (d) but computed from simulations reported in (e). (h), (i) Same as (f) and (g) but including noise and finite bandwidth effects in the heterodyne measurement, see Supplemental Material [44] for details.

spectral support of the DOS in the upper complex plane, reshaping the vertical linear support of the initial Weyl distribution into a semicircular one. It is important to note that the concept of a circular spectral support for the DOS of a SG was introduced mathematically in Ref. [18], but without any expectation that this class of SGs could be observed experimentally nor that it could emerge from a nonintegrable evolution. It is also worth noting that our experiments demonstrate a transition from a soliton condensate to a circular SG, rather than to a circular condensate.

As shown in Figs. 2(f) and 2(g), the dissipation-driven changes of the geometrical support of the DOS are also found in numerical simulations of Eq. (1) that are made with the experimental parameters. It is noteworthy that the DOS obtained from numerical simulations of Eq. (1), shown in Fig. 2(f), exhibits a perfectly symmetric shape that is not found in the experiments, as seen in Fig. 2(c). This slight discrepancy between the experimental and numerical DOS, along with the blurrier appearance of the experimental DOS, is attributed to noise and finite bandwidth effects in the heterodyne measurement of the optical field's phase and amplitude, as illustrated in Figs. 2(h) and 2(i) and discussed in more detail in Supplemental Material [44]. Let us also emphasize that, with the constant loss rate, the optical SG never attains a steady state and the circular support of the DOS continuously undergoes homothetic evolution; see the Supplemental Material [44] for more details on the DOS evolution.

Next, we examine another dissipative experiment in which the optical SG undergoes a linearly amplified evolution instead of a damped one. Increasing the power of the 1450 nm pump laser, we now consider a situation in which the mean optical power of the SG increases from ~2 mW to ~4 mW over ~6300 km, as shown in Fig. 3(a). Figure 3(b) reveals that the space-time evolution of the optical SG looks qualitatively different from the situation with damping reported in Fig. 2(b). Following the initial destabilization of the flat-top pulse, individual nonlinear structures with small relative velocities are observed to form and persist within the fiber loop. At a qualitative level, the observed space-time evolution shows remarkable similarities to that reported in previous numerical studies on growing IT, even though these studies considered a completely different initial condition [36].

Figures 3(c) and 3(d) illustrate that the DOS of the SG, initially in the form of the Weyl distribution, essentially evolves into two distinct clustered distributions. One of these clusters is centered around $\lambda_0 \simeq 1.8i$, while the other is centered around $\lambda_1 \simeq 0.3i$. Here, the statistical computation of the DOS involves an ensemble of ~10 700 (resp. ~12 100) discrete eigenvalues at $z = 0$ km (resp. $z = 6320$ km). The fact that $\text{Re}(\lambda_0) \sim \text{Re}(\lambda_1) \sim 0$ is the spectral signature of all solitons in the amplified SG exhibiting small velocities, in stark contrast to the scenario depicted in Fig. 2(c), where damping was shown to broaden the soliton velocity distribution. The difference between $\text{Im}(\lambda_0) \simeq 1.8$ and $\text{Im}(\lambda_1) \simeq 0.3$ indicates that the SG formed at $z \sim 6300$ km is predominantly composed of two distinct species, characteristic of a bichromatic SG [17,32].

Figure 3(e) shows that the space time evolution observed in the experiment is well reproduced by numerical simulations of Eq. (1) for $\alpha_{\text{eff}} \sim -1.1 \times 10^{-4}$ km^{-1}, corresponding to $\epsilon = -0.042$. Figures 3(f)–3(i) show that the features observed experimentally in terms of evolution of the DOS are also found in numerical simulations that include noise and finite bandwidth effects due to the heterodyne measurement of the optical field's phase and amplitude, see Supplemental Material [44] for details.

In our experiments, dissipation significantly alters the mass $M(t) = \int_{-\infty}^{+\infty} |\psi(x,t)|^2 dx$, or equivalently, the mean power, $P(z) = \int_{-\infty}^{+\infty} |A(T,z)|^2 dT$, of the optical SG, see Figs. 2(a) and 3(a). However, the total number of discrete eigenvalues, $N(z)$, does not vary in proportion to the changes in mass. In Fig. 2(a) the mass decreases by a factor ∼6, while N changes by only ∼20% during the evolution. Similarly, in Fig. 3(a), the mass approximately doubles but N changes by only 10% during the evolution. This indicates that the changes in the mass of the optical SGs are not primarily caused by the creation or annihilation of soliton states, but rather by the rearrangement of the DOS in the upper complex plane.

To substantiate this point in a more quantitative way, we consider the expression of the mass of SG given by the spectral kinetic theory:

$$M = 4\int_0^{+\infty} \eta \tilde{f}(\eta) d\eta = \int_0^{+\infty} \rho(\eta) d\eta, \tag{4}$$

where $\tilde{f}(\eta) = \int_{-\infty}^{+\infty} d\xi f(\xi,\eta)$ represents the DOS $f(\xi,\eta)$ that has been integrated over the real axis ξ [18,19]. $\rho(\eta) = 4\eta\tilde{f}(\eta)$ represents the spectral density of mass with respect to η.

Figure 4(a) illustrates that the spectral density of mass, $\rho(\eta)$, for the initial bound-state SG closely matches the spectral density $\rho_W(\eta) = 4\eta f_W(\eta)$, which corresponds to the Weyl distribution. In contrast, Fig. 4(b) shows how experimental damping significantly alters $\rho(\eta)$, transforming it into a bell-shaped distribution centered around $\eta \simeq 0.4$ (green histogram). On the other hand, linear amplification of the SGs results in the development of an asymmetric distribution of the spectral density [gray histogram in Fig. 4(b)], with its peak shifted to approximately $\eta \simeq 1.8$. The mass associated with the cluster of eigenvalues centered around $\lambda_1 \simeq 0.3i$ constitutes only a few percent of the total mass of the formed bichromatic SG, see Supplemental Material [44] for details.

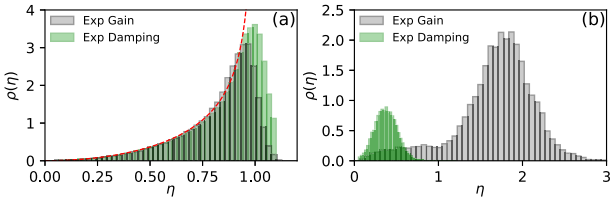

FIG. 4. Experimental histograms showing the spectral density of mass, $\rho(\eta)$, along the vertical imaginary axis η. (a) The green (resp. gray) histogram represents the initial distribution in the experiment with linear damping (resp. amplification) of the SG. The red dashed line represents the spectral density of mass $\rho_W(\eta) = 4\eta f_W(\eta)$ associated with the Weyl distribution $f_W(\eta) = \eta/(\pi\sqrt{1-\eta^2})$. (b) Same as (a) but at $z \sim 1920$ km (green histogram) and $z \sim 6320$ km (gray histogram).

In conclusion, we have presented optical fiber experiments exploring the perturbed evolution of SGs under the influence of small linear damping and gain. Our experiments reveal that dissipation-induced changes in the mass (equivalently, in the mean power) of optical SGs are predominantly driven by a redistribution of the DOS in the upper complex plane, rather than by the creation or annihilation of soliton states. This feature contrasts with recent findings in the perturbed evolution of KdV SGs, see Ref. [34]. Previous studies investigating dissipative evolution in NLS systems have primarily focused on ensembles containing only a few solitons, employing approaches such as numerical simulations or perturbed IST theory [52–56]. We hope that our experiments, which explore large ensembles of interacting solitons with random characteristics, will inspire theoretical investigations using GHD, possibly building on previous studies of one-dimensional Bose gases with atom losses [57,58]. Furthermore, our experiments demonstrate that higher-order perturbative effects can be exploited to manipulate the spectral (IST) characteristics of SGs, offering new experimental opportunities.

Acknowledgments—We thank Dmitry Agafontsev, Thibault Bonnemain, Thibault Congy, Gennady El, Andrey Gelash, Giacomo Roberti, and Alexander Tovbis for their collaboration and the discussions we have had over the years on SG-related topics. This work has been partially supported by the Agence Nationale de la Recherche through the SOGOOD (ANR-21-CE30-0061) projects, the LABEX CEMPI project (ANR-11-LABX-0007), the Ministry of Higher Education and Research, Hauts de France council and European Regional Development Fund (ERDF) through the Nord-Pas de Calais Regional Research Council and the European Regional Development Fund (ERDF) through the Contrat de Projets Etat-Région (CPER Photonics for Society P4S). The authors would like to thank the Centre d'Etudes et de Recherche Lasers et Application (CERLA) for technical support and the Isaac Newton Institute for Mathematical Sciences, Cambridge, for support and hospitality during the programme Emergent phenomena in nonlinear dispersive waves, where work on this Letter was undertaken.

Data availability—The data that support the findings of this article are not publicly available. The data are available from the authors upon reasonable request.

[1] V. E. Zakharov, Stud. Appl. Math. **122**, 219 (2009).
[2] J. M. Soto-Crespo, N. Devine, and N. Akhmediev, Phys. Rev. Lett. **116**, 103901 (2016).
[3] I. Redor, H. Michallet, N. Mordant, and E. Barthélemy, Phys. Rev. Fluids **6**, 124801 (2021).
[4] S. Randoux, P. Walczak, M. Onorato, and P. Suret, Phys. Rev. Lett. **113**, 113902 (2014).

[5] G. Michel, F. Bonnefoy, G. Ducrozet, G. Prabhudesai, A. Cazaubiel, F. Copie, A. Tikan, P. Suret, S. Randoux, and E. Falcon, Phys. Rev. Fluids **5**, 082801(R) (2020).

[6] T. Congy, G. A. El, G. Roberti, A. Tovbis, S. Randoux, and P. Suret, Phys. Rev. Lett. **132**, 207201 (2024).

[7] S. Randoux, F. Gustave, P. Suret, and G. El, Phys. Rev. Lett. **118**, 233901 (2017).

[8] D. S. Agafontsev and V. E. Zakharov, Nonlinearity **28**, 2791 (2015).

[9] Z.-Y. Sun, X. Yu, and Y.-J. Feng, Phys. Rev. E **108**, 054211 (2023).

[10] S. Nazarenko, *Wave Turbulence*, Lecture Notes in Physics (Springer, Berlin, Heidelberg, 2011).

[11] A. Picozzi, J. Garnier, T. Hansson, P. Suret, S. Randoux, G. Millot, and D. Christodoulides, Phys. Rep. **542**, 1 (2014).

[12] E. Falcon and N. Mordant, Annu. Rev. Fluid Mech. **54**, 1 (2022).

[13] S. Galtier, *Physics of Wave Turbulence* (Cambridge University Press, Cambridge, England, 2022).

[14] P. G. Drazin and R. S. Johnson, *Solitons: An Introduction* (Cambridge University Press, Cambridge, England, 1989), Vol. 2.

[15] M. Ablowitz, *Nonlinear Dispersive Waves: Asymptotic Analysis and Solitons*, Cambridge Texts in Applied Mathematics (Cambridge University Press, Cambridge, England, 2011).

[16] V. E. Zakharov, Sov. Phys. JETP **33**, 538 (1971).

[17] G. A. El and A. M. Kamchatnov, Phys. Rev. Lett. **95**, 204101 (2005).

[18] G. El and A. Tovbis, Phys. Rev. E **101**, 052207 (2020).

[19] G. A. El, J. Stat. Mech. (2021) 114001.

[20] P. Suret, S. Randoux, A. Gelash, D. Agafontsev, B. Doyon, and G. El, Phys. Rev. E **109**, 061001 (2024).

[21] R. Koch, J.-S. Caux, and A. Bastianello, J. Phys. A **55**, 134001 (2022).

[22] T. Bonnemain, B. Doyon, and G. El, J. Phys. A **55**, 374004 (2022).

[23] B. Bertini, M. Collura, J. De Nardis, and M. Fagotti, Phys. Rev. Lett. **117**, 207201 (2016).

[24] O. A. Castro-Alvaredo, B. Doyon, and T. Yoshimura, Phys. Rev. X **6**, 041065 (2016).

[25] B. Doyon, S. Gopalakrishnan, F. Møller, J. Schmiedmayer, and R. Vasseur, Phys. Rev. X **15**, 010501 (2025).

[26] I. Redor, E. Barthélemy, H. Michallet, M. Onorato, and N. Mordant, Phys. Rev. Lett. **122**, 214502 (2019).

[27] A. Costa, A. R. Osborne, D. T. Resio, S. Alessio, E. Chrivì, E. Saggese, K. Bellomo, and C. E. Long, Phys. Rev. Lett. **113**, 108501 (2014).

[28] S. M. Mossman, G. C. Katsimiga, S. I. Mistakidis, A. Romero-Ros, T. M. Bersano, P. Schmelcher, P. G. Kevrekidis, and P. Engels, Commun. Phys. **7**, 163 (2024).

[29] G. Marcucci, D. Pierangeli, A. J. Agranat, R.-K. Lee, E. DelRe, and C. Conti, Nat. Commun. **10**, 5090 (2019).

[30] P. Suret, A. Tikan, F. Bonnefoy, F. Copie, G. Ducrozet, A. Gelash, G. Prabhudesai, G. Michel, A. Cazaubiel, E. Falcon, G. El, and S. Randoux, Phys. Rev. Lett. **125**, 264101 (2020).

[31] L. Dieli, D. Pierangeli, E. DelRe, and C. Conti, Phys. Rev. Lett. **133**, 183801 (2024).

[32] L. Fache, F. Bonnefoy, G. Ducrozet, F. Copie, F. Novkoski, G. Ricard, G. Roberti, E. Falcon, P. Suret, G. El, and S. Randoux, Phys. Rev. E **109**, 034207 (2024).

[33] P. Suret, M. Dufour, G. Roberti, G. El, F. Copie, and S. Randoux, Phys. Rev. Res. **5**, L042002 (2023).

[34] L. Fache, H. Damart, F. Copie, T. Bonnemain, T. Congy, G. Roberti, P. Suret, G. El, and S. Randoux, Phys. Rev. Lett. **134**, 147201 (2025).

[35] D. S. Agafontsev and V. E. Zakharov, Low Temp. Phys. **46**, 786 (2020).

[36] D. S. Agafontsev, A. A. Gelash, R. I. Mullyadzhanov, and V. E. Zakharov, Chaos Solitons Fractals **166**, 112951 (2023).

[37] F. Coppini, P. G. Grinevich, and P. M. Santini, Phys. Rev. E **101**, 032204 (2020).

[38] A. E. Kraych, P. Suret, G. El, and S. Randoux, Phys. Rev. Lett. **122**, 054101 (2019).

[39] A. E. Kraych, D. Agafontsev, S. Randoux, and P. Suret, Phys. Rev. Lett. **123**, 093902 (2019).

[40] A. Gelash, D. Agafontsev, V. Zakharov, G. El, S. Randoux, and P. Suret, Phys. Rev. Lett. **123**, 234102 (2019).

[41] F. Bonnefoy, A. Tikan, F. Copie, P. Suret, G. Ducrozet, G. Prabhudesai, G. Michel, A. Cazaubiel, E. Falcon, G. El, and S. Randoux, Phys. Rev. Fluids **5**, 034802 (2020).

[42] G. A. El, E. G. Khamis, and A. Tovbis, Nonlinearity **29**, 2798 (2016).

[43] R. Mullyadzhanov and A. Gelash, Phys. Rev. Lett. **126**, 234101 (2021).

[44] See Supplemental Material at http://link.aps.org/supplemental/10.1103/hwpr-628r; for details about the experimental setup, the experimental methodology, the evolution of the DOS in experiment and in numerical simulations.

[45] S. Toenger, T. Godin, C. Billet, F. Dias, M. Erkintalo, G. Genty, and J. M. Dudley, Sci. Rep. **5**, 10380 (2015).

[46] M. Närhi, B. Wetzel, C. Billet, S. Toenger, T. Sylvestre, J.-M. Merolla, R. Morandotti, F. Dias, G. Genty, and J. M. Dudley, Nat. Commun. **7**, 13675 (2016).

[47] P. Suret, R. El Koussaifi, A. Tikan, C. Evain, S. Randoux, C. Szwaj, and S. Bielawski, Nat. Commun. **7**, 13136 (2016).

[48] O. Kimmoun, H. Hsu, H. Branger, M. Li, Y. Chen, C. Kharif, M. Onorato, E. J. Kelleher, B. Kibler, N. Akhmediev *et al.*, Sci. Rep. **6**, 28516 (2016).

[49] J. M. Dudley, G. Genty, A. Mussot, A. Chabchoub, and F. Dias, Nat. Rev. Phys. **1**, 675 (2019).

[50] G. Vanderhaegen, P. Szriftgiser, A. Kudlinski, M. Conforti, A. Armaroli, and A. Mussot, Phys. Rev. A **106**, 033519 (2022).

[51] J. Yang, Nonlinear Waves in Integrable and Non-integrable Systems, Mathematical Modeling and Computation (Society for Industrial and Applied Mathematics, Philadelphia, 2010).

[52] K. J. Blow, N. J. Doran, and D. Wood, J. Opt. Soc. Am. B **5**, 381 (1988).

[53] T. Okamawari, A. Hasegawa, and Y. Kodama, Phys. Rev. A **51**, 3203 (1995).

[54] J. E. Prilepsky and S. A. Derevyanko, Phys. Rev. E **75**, 036616 (2007).

[55] M. Böhm and F. Mitschke, Phys. Rev. A **76**, 063822 (2007).

[56] A. Hause, C. Mahnke, and F. Mitschke, Phys. Rev. A **98**, 033814 (2018).

[57] I. Bouchoule, B. Doyon, and J. Dubail, SciPost Phys. **9**, 044 (2020).

[58] I. Bouchoule and J. Dubail, Phys. Rev. Lett. **126**, 160603 (2021).